

Quantitative techniques for musculoskeletal MRI at 7 Tesla

Neal K. Bangerter^{1,2}, Meredith D. Taylor¹, Grayson J. Tarbox¹, Antony J. Palmer³, Daniel J. Park³

¹Department of Electrical & Computer Engineering, Brigham Young University, Provo, UT, USA; ²Department of Radiology, University of Utah, Salt Lake City, UT, USA; ³Department of Orthopaedics, University of Oxford, Oxford, UK

Correspondence to: Neal K. Bangerter, PhD. Department of Electrical & Computer Engineering, Brigham Young University, Provo, UT, USA.
Email: nealb@ee.byu.edu.

Abstract: Whole-body 7 Tesla MRI scanners have been approved solely for research since they appeared on the market over 10 years ago, but may soon be approved for selected clinical neurological and musculoskeletal applications in both the EU and the United States. There has been considerable research work on musculoskeletal applications at 7 Tesla over the past decade, including techniques for ultra-high resolution morphological imaging, 3D T2 and T2* mapping, ultra-short TE applications, diffusion tensor imaging of cartilage, and several techniques for assessing proteoglycan content in cartilage. Most of this work has been done in the knee or other extremities, due to technical difficulties associated with scanning areas such as the hip and torso at 7 Tesla. In this manuscript, we first provide some technical context for 7 Tesla imaging, including challenges and potential advantages. We then review the major quantitative MRI techniques being applied to musculoskeletal applications on 7 Tesla whole-body systems.

Keywords: 7 Tesla; magnetic resonance imaging; musculoskeletal; quantification; knee; extremities

Submitted Nov 27, 2016. Accepted for publication Dec 15, 2016.

doi: 10.21037/qims.2016.12.12

View this article at: <http://dx.doi.org/10.21037/qims.2016.12.12>

Introduction

Several major MRI vendors have, over the past decade, made available 7 Tesla whole body scanners. These scanners are generally not yet approved for clinical use, but have garnered significant interest at research institutions due to the promise of better image quality from the higher field strength (resulting in a stronger MR signal). Many major research institutions with large magnetic resonance imaging research programs have acquired these 7 Tesla whole body scanners, but, due to a variety of challenges that will be discussed below, the eventual clinical utility of such systems had been unclear. However, in May of 2015, Siemens Healthcare became the first major MRI vendor to announce a 7 Tesla platform targeted for clinical application, stating that the system “is the world’s first ultra-high field research system ready for future clinical use with planned CE and FDA authorization to market for selected neurological and musculoskeletal MR imaging applications” (1).

Given the promise of a 7 Tesla whole body system with

planned CE (European Union) and FDA (United States) authorization for musculoskeletal MR imaging applications, we aim to provide in this review a high-level overview of some of these musculoskeletal applications, with a specific focus on quantitative imaging techniques. We first provide some technical context for 7 Tesla imaging, and the advantages and challenges associated with this high main polarizing field strength *vs.* lower field strengths (1.5/3 Tesla). We then review the major quantitative MRI techniques being applied to musculoskeletal applications on 7 Tesla whole-body systems. We conclude by making the case that 7 Tesla quantitative musculoskeletal MRI could indeed provide significant advantages over lower field strengths for certain body areas (e.g., the knee and extremities) and certain applications (e.g., assessment of proteoglycan content in cartilage, detection of small morphological changes in cartilage over time). However, we feel the case for 7 Tesla is much less compelling for other areas, such as the torso and hip.

Technical considerations

Relationship between field strength and SNR

The nuclear magnetic resonance (NMR) signal from the ^1H (hydrogen) nucleus is the signal typically detected to form an MRI image. The NMR signal is a radiofrequency (RF) wave whose amplitude is linearly proportional to the net magnetic polarization of the hydrogen nuclei in the material being imaged. This net magnetic polarization scales linearly with the magnetic field strength of the MRI machine. In simple terms, this means that a 3 Tesla MRI machine will yield an NMR signal that is twice as strong as a 1.5 Tesla MRI machine, all else being equal. The noise in the NMR signal is expected to be roughly equal at both field strengths, implying that a doubling of field strength (from 1.5 to 3 Tesla) could theoretically yield a doubling of signal-to-noise ratio (SNR, a common technical measure of image quality). While other factors and non-idealities make this doubling of SNR from 1.5 to 3 Tesla difficult to achieve in practice, a significant boost in SNR is still typically observed, making higher field strength MRI machines an attractive option.

The higher inherent signal at higher field strengths can be exploited in a variety of ways. It can be translated into higher SNR for imaging at a given field of view (FOV), voxel size, and scan time. Alternately, it can in some cases be used to reduce scan time while preserving image SNR for a given FOV and voxel size. Finally, it can be used to offset some of the SNR loss associated with going to higher resolutions, potentially allowing images at higher resolutions and higher SNR than could be obtained in similar scan times at lower field strength.

With this in mind, moving from a main polarizing field strength of 3 Tesla to 7 Tesla could theoretically provide a more than doubling of signal SNR (all else being equal). This potential has largely motivated the research demand for ultra-high field (7 Tesla) whole body scanners. However, there are a variety of new challenges that become much more acute at main polarizing field strengths of 7 Tesla *vs.* 1.5 and even 3 Tesla. We describe these below.

Radiofrequency considerations: tissue heating

An important consideration in MRI is radiofrequency power deposition; the RF energy transmitted by the MRI machine for excitation of the NMR signal causes tissue heating. RF power deposition is described by a quantity known as specific absorption rate (SAR), measured in Watts

per kilogram (W/kg). The power deposited in tissue by a radiofrequency wave scales roughly quadratically with frequency for an RF pulse of the same amplitude and duration, while the RF frequencies present in MRI scale linearly with field strength (2). Tissue heating is thus a much larger concern at higher field strengths.

Further compounding the tissue heating problem at 7 Tesla is the much shorter wavelength of the involved RF waves in tissue. At 3 Tesla, the RF wavelengths in many tissues are ~ 35 cm, whereas at 7 Tesla these drop to ~ 15 cm. When the wavelength becomes comparable to or smaller than the anatomy being imaged, several problems result. First, the RF waves have a more difficult time penetrating the body (so-called “skin depth effects”), leading to a high degree of inhomogeneity in flip angle across the anatomy being imaged (known as “transmit B1 inhomogeneity”). Higher RF transmit powers are then needed to achieve a desired flip angle deep in the tissue being imaged, potentially increasing RF power deposition and tissue heating to dangerous levels across large sections of the body. This makes it impractical (and potentially dangerous) to use the large body RF transmit coils typical for 1.5 Tesla and 3 Tesla systems on 7 Tesla whole body scanners.

On 1.5 and 3 Tesla systems, the body RF transmit coil is almost always used for signal excitation, and provides a relatively homogeneous flip angle across even quite large fields of view. At 7 Tesla, a body coil could not provide a homogeneous flip angle across even much smaller fields of view, and could induce significant heating across the body being imaged. The lack of a body RF coil on 7 Tesla whole body scanners leads to some significant constraints on what can reasonably be imaged on ultra-high field scanners. As previously mentioned, at lower fields the body RF coil is typically used for excitation. Smaller local coils or arrays of coils are then often used for signal reception. At 7 Tesla, RF coil configurations must be used that can both excite and receive the RF signal. Even these smaller excitation coils can pose significant challenges. To penetrate deep into large sections of the body, transmit RF phased arrays are being explored. However, the shorter wavelengths at higher fields can lead to constructive and destructive RF wave interference patterns in the body (from the transmit array) that are very difficult to model and predict, potentially leading to RF “hot spots” that could cause excessive tissue heating or even burning in localized areas. Modeling the RF heating patterns from transmit coil configurations such as these is a major safety consideration for 7 Tesla MRI, and an area of considerable research activity.

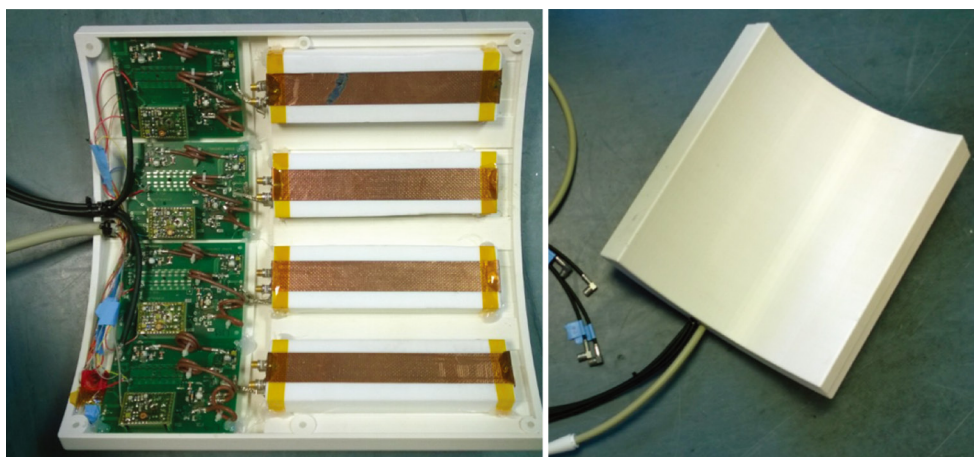


Figure 1 Custom four-channel parallel transmit/receive phased array coil for hip imaging at 7 Tesla. Since 7 Tesla whole body scanners lack a body RF coil for signal excitation, coil configurations must be able to both excite and receive the NMR signal. However, the short wavelength of the NMR signal at 7 Tesla makes coil design much more challenging. Furthermore, the field patterns in the human body induced during excitation by a transmit phased-array must be accurately modeled to ensure that the coil will not create local hotspots in the scan subject, potentially leading to internal burns. (Image used courtesy of the Department of Orthopaedics, University of Oxford).

Effective imaging of many parts of the body, such as the human torso and hips, requires these transmit phased arrays at 7 Tesla. A prototype of one such 4-channel parallel transmit/receive coil is shown in *Figure 1*, designed for use on a Siemens 7 Tesla system at the University of Oxford. Unfortunately, the RF modeling to demonstrate safety from a tissue heating perspective for such a coil is extremely difficult. For this reason, the vast majority of the work being done at 7 Tesla has focused on areas of the body that can be surrounded by smaller transmit birdcage-type coils (whose tissue heating characteristics are easier to model), such as the head and extremities. Much of the musculoskeletal work at 7 Tesla has focused primarily on the knee or other peripheral joints, and to a lesser degree superficial anatomical features that can be easily imaged with a small transmit/receive surface coil.

Flip angle (transmit B1) and receive sensitivity inhomogeneity

In addition to the high degree of transmit B1 (or flip angle) inhomogeneity typical of 7 Tesla RF transmit coil configurations, significant inhomogeneity in receive coil spatial sensitivity is also typical. These two factors (inhomogeneous flip angle across the volume, and inhomogeneous signal detection across the volume) combine to make extraction of certain quantitative parameters much more challenging at 7 Tesla. Accurate measurement of

many tissue properties in MRI relies on accurate knowledge of both the flip angle and receive sensitivity at the voxel in question. At lower fields, the use of the relatively homogeneous body coil for signal transmit means that flip angle is typically known across the volume. Receive coil sensitivity maps are still often needed, but the variations are often small across a volume of interest. At 7 Tesla, the flip angle can vary significantly across the volume being imaged, as can the receive sensitivity. For quantitative estimation of certain tissue characteristics, accurate flip angle and receive sensitivity maps are essential, and often more difficult to accurately acquire than at lower field strengths.

Main field (B0) inhomogeneity

Finally, many pulse sequences in MRI are sensitive to variations in the main polarizing field (the B0 field) across a volume being imaged. Warping of the polarizing magnetic field due to boundaries between tissues of different magnetic susceptibilities is proportional to field strength. A 3 parts per million (ppm) variation in the magnetic field at 7 Tesla corresponds to an 894 Hz shift in resonant frequency, while the same 3 ppm shift at 3 Tesla corresponds to a 384 Hz shift in frequency. The same is true for chemical shift, such as the shift in resonance for hydrogen in lipids *vs.* water. Sequences that are sensitive to B0 inhomogeneity will typically have even more challenges at higher field strengths.

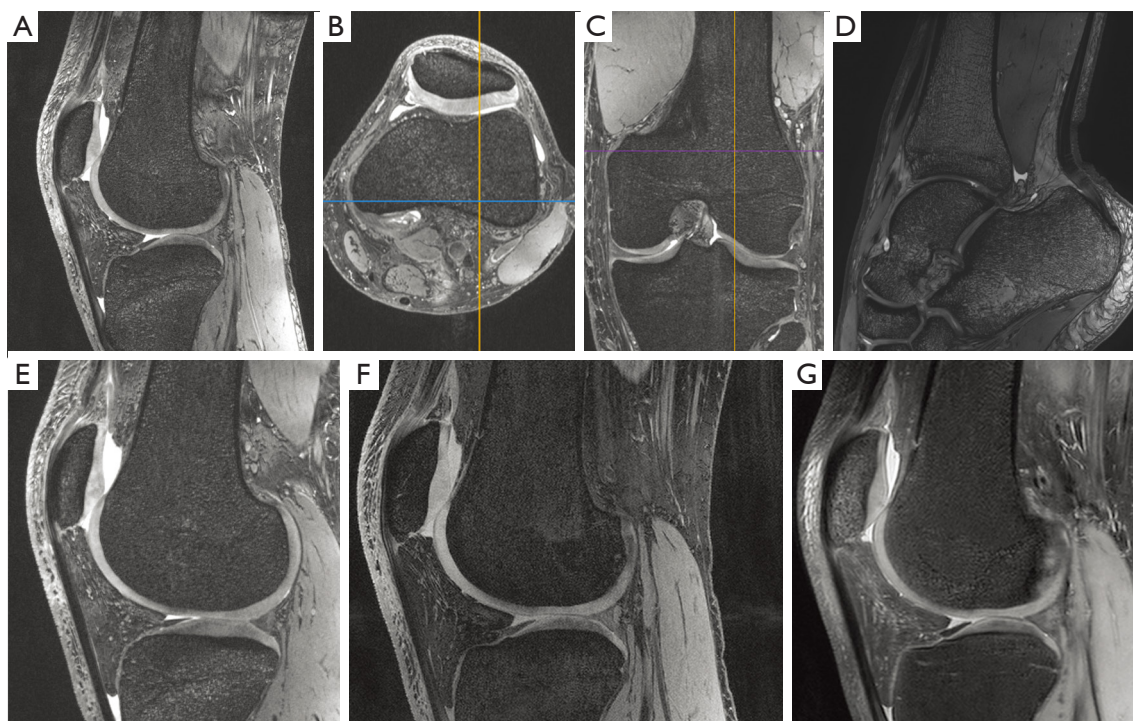


Figure 2 Ultra-high resolution 3D images of the human knee in vivo at 7 Tesla. A phase-cycled balanced SSFP sequence achieving isotropic 0.3 mm resolution in just under 9 minutes of scan time in the knee using a 28-channel knee coil is shown formatted in the sagittal (A), axial (B), and coronal (C) planes. A single slice from a similar sequence applied in the ankle is shown in (D). A sagittal knee is shown in (E-G) using three different morphological 3D sequences. Phase-cycled balanced SSFP at 0.3 mm isotropic resolution and 8 min 50 sec scan time is shown in (E), a 3D water-excitation DESS sequence at 0.36 mm isotropic resolution and 6 min 54 sec scan time is shown in (F), and a 3D SPACE scan at 0.55 mm isotropic resolution and 11 min 37 sec scan time (G). (Images used courtesy of the Department of Orthopaedics, University of Oxford.)

Techniques for quantitative imaging at 7 Tesla for MSK applications

Ultra-high resolution morphological imaging

Quantitative cartilage volume and thickness measurements across regions and subregions of a joint are increasingly used as outcome measures in longitudinal studies of osteoarthritis. A standard knee-imaging protocol at 3 Tesla was introduced for the Osteoarthritis Initiative (OAI), a massive longitudinal study that has followed a cohort of over 4,500 individuals over four years (3). Data from this study has been used to develop a series of morphological measurement techniques, and certain standards for segmentation and measurement are beginning to emerge. The protocol has since been adopted for other clinical trials related to development and progression of osteoarthritis in the knee. The OAI knee protocol acquires two separate high resolution 3D full knee scans, one using a standard 3D

DESS protocol (~10 minutes for full knee coverage), and one a standard 3D FLASH (also ~10 minutes).

The authors (Palmer, Bangerter, and Park) adapted the 3D DESS scan from the OAI for use at 7 Tesla, and then developed an even higher resolution phase-cycled bSSFP protocol (using two phase cycles combined with sum-of-squares) that took roughly the same amount of time (10 minutes). We further developed a high-resolution 3D protocol using a Siemens work-in-progress (WIP) 3D SPACE sequence. While segmentations have not yet been performed on this data to assess the accuracy and repeatability of measurement, sample images are shown in *Figure 2*. The resolution and level of detail achievable using these various 3D sequences is very promising.

Assessment of trabecular bone microarchitecture

Regatte, Chang, and colleagues at New York University

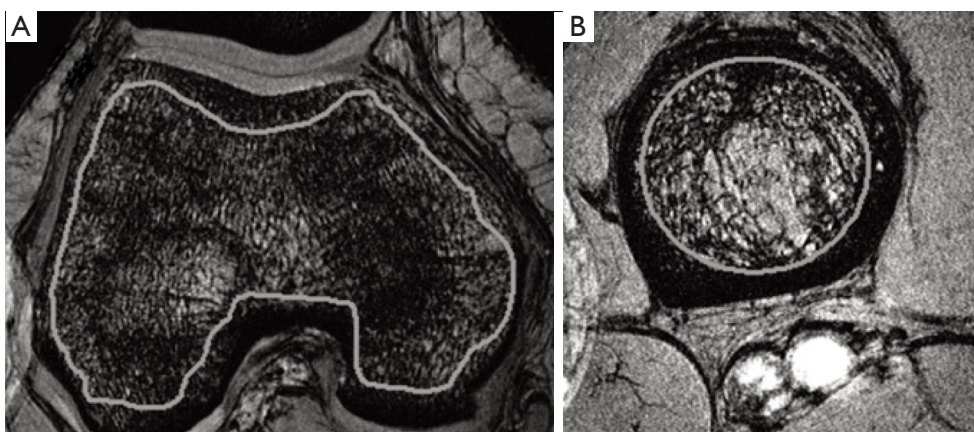


Figure 3 Regatte, Chang, and colleagues at New York University used a 3D Flash sequence at 7T to assess trabecular bone microarchitecture (4). Quantitative measure of both bone volume fraction and marrow volume fraction in the knee were obtained by first segmenting the trabecular bone from surrounding tissues, and then estimating fraction from the signal-producing marrow *vs.* the non-signal-producing bone across the segmented region of interest. Segmentation of the femoral condyles is shown in (A) and in the proximal tibia in (B). (Copyright 2008 Wiley. Used with permission from Chang G, Pakin SK, Schweitzer ME, Saha PK, Regatte RR. Adaptations in trabecular bone microarchitecture in Olympic athletes determined by 7T MRI, *Journal of Magnetic Resonance Imaging*, John Wiley & Sons.)

have investigated the use of a standard high-resolution 3D Flash sequence at 7T to assess trabecular bone microarchitecture (4-6). Quantitative measure of both bone volume fraction and marrow volume fraction in the knee and hip were obtained by first segmenting the trabecular bone from surrounding tissues, and then estimating fraction from the signal-producing marrow *vs.* the non-signal-producing bone across the segmented region of interest. *Figure 3* shows example images of the femoral condyles (A) and proximal tibia (B). They found these measures to be both feasible and highly reproducible.

T2 and T2* mapping

T2 mapping has been shown to correlate with both cartilage collagen matrix integrity and water content (7), and is useful for evaluating disease progression in osteoarthritis, cartilage hydration, or assessing damage or cartilage health after physical trauma to a joint or interventional surgery. Absolute T2 values are affected by both free and bound water (7). When there is an increase in free water (often associated with breakdown of the collagen matrix in cartilage) an increase in T2 is typically observed.

Trattinig, Welsch, and colleagues at the University of Vienna used a standard multi-echo spin-echo (MESE) T2 mapping sequence and a multi-echo GRE T2* mapping sequence at 7 Tesla for imaging knee cartilage, and

compared the results with similar sequences at 3 Tesla (8). The cartilage maps at both 3 Tesla and 7 Tesla were segmented by three separate observers, and zonal and subregion analyses of T2 and T2* performed by each observer. A coefficient of variation was calculated and used as a measure of reproducibility. The measurements were found to be more consistent across observers (1.3–1.5% lower coefficient of variation depending on the region of cartilage analyzed) using the 7 Tesla data *vs.* the 3 Tesla data. This is most likely due to the increase in SNR at 7T.

Kraff, Lazik, and colleagues in Essen and Heidelberg, Germany developed a 7 Tesla 2D protocol for T2 and T2* mapping of hip cartilage (9). A custom in-house developed 8-channel transmit/receive hip array was used for imaging. T2 mapping was performed with similar sequences to the Vienna group, using MESE for T2 mapping and multi-echo GRE for T2* mapping. T2 and T2* mapping of hip cartilage at lower field strengths (1.5 and 3 Tesla) is confounded by the very thin cartilage surfaces on the femoral head and acetabulum, leading to partial volume effects from surrounding tissues. They were able to achieve higher resolution (5 slices at 0.5 mm × 0.5 mm in plane resolution with 2.5 mm thick slices) than previous studies at 3 Tesla in clinically reasonable scan times at 7 Tesla (under 5 minutes for the T2 map, T2* maps in under 2 minutes), and found that the increased resolution gained by going to 7 Tesla was essential to mitigate partial volume contamination

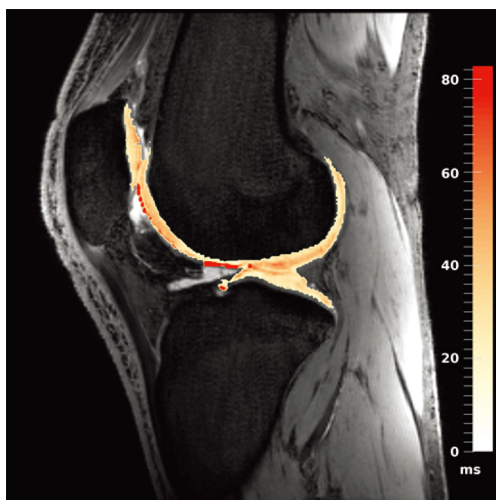


Figure 4 High-resolution 3D cartilage T2 map obtained using a 3D modified DESS sequence overlaid on a sagittal bSSFP image. Sequences such as the modified 3D DESS shown here enable the simultaneous acquisition of high-resolution morphological data and accurate 3D T2 maps. These sequences are expected to be much better suited to T2 mapping at 7 Tesla than the standard 2D multi-echo spin echo (MESE) techniques employed at lower field strengths due to the high B1 inhomogeneity on 7 Tesla systems, although further work is needed to verify. (Image used courtesy of the Department of Orthopaedics, University of Oxford.)

of T2 and T2* maps of hip cartilage that were observed at 3 Tesla.

Additional work in assessing surgically repaired cartilage tissue with 7 Tesla 2D MESE T2 mapping was been performed by Chang *et al.* at New York University and Domayer *et al.* at the University of Vienna. Both groups performed studies comparing restored cartilage to adjacent cartilage (6,10), and both found a significant difference in T2 values between regions of adjacent healthy cartilage and repaired cartilage. Both groups had experienced readers segment repaired and adjacent healthy cartilage for comparison. The University of Vienna group found T2 values of healthy ankle cartilage of 31.4 ± 3.1 ms and repaired cartilage of 39.8 ± 8.6 ms which they concluded is a statistically significant difference ($P=0.009$). The New York University group found healthy knee cartilage T2 values of 51.6 ± 7.6 and repaired cartilage of 40.0 ± 4.7 , also a statistically significant difference ($P=0.0005$).

Kraff *et al.* (Essen, Germany) and Juras *et al.* (University of Vienna) used a novel 3D-TESS (three steady-state free

precession) technique to create higher resolution 3D T2 maps, rather than the standard 2D MESE technique (11,12). This had the advantage of lowering SAR (lower tissue heating), and allows higher resolutions and/or increased volume coverage in a true 3D scan. Kraff and colleagues performed T2 maps using the same resolution for both the novel TESS method as well as the standard MESE technique ($0.5 \text{ mm} \times 0.5 \text{ mm} \times 2.5 \text{ mm}$), but they achieved much better coverage using the TESS method (32 slices) than the MESE method (6 slices). They also found that this method is less sensitive to B1 inhomogeneity and thus was more reproducible. The University of Vienna group was able to achieve a resolution of $0.5 \text{ mm} \times 0.5 \text{ mm} \times 3 \text{ mm}$ with 22 slices in only 1 minute 37 seconds.

Work from the authors at the University of Oxford demonstrated the use of a 7 Tesla 3D quantitative modified DESS scan (13) that allows the extraction of T2 maps in addition to providing excellent morphological data. *Figure 4* shows a sagittal T2 map of the knee obtained using the sequence on a 7 Tesla Siemens scanner with a 28-channel knee coil, with the computed cartilage T2 map overlaid on the morphological image. The images were acquired in 3D across the entire knee at a resolution of $0.63 \text{ mm} \times 0.63 \text{ mm} \times 2 \text{ mm}$ in an acquisition time of 8 minutes. These maps appear qualitatively to be quite accurate, exhibiting the relatively smooth variations across cartilage one would expect when a good fit is achieved in adjacent pixels across the cartilage (i.e., very little apparent noise is present across the cartilage T2 estimates in the maps). However, these techniques are very new, and quantitative comparison of the performance of these new 3D steady-state T2 mapping techniques at high field *vs.* traditional 2D multi-echo spin echo maps or against steady state techniques at lower field are still needed.

Ultrashort echo time (UTE) T2 mapping*

Certain tissues, like tendon and bone, exhibit T2* decay that is so rapid (typical T2* values of 10s of microseconds up to several milliseconds) that it is impractical to use normal T2* mapping techniques. The signal from these tissues simply decays away too quickly to capture with normal sequences. In these cases, so-called ultrashort echo time (UTE) sequences are used, where the signal is sampled very rapidly after excitation. These sequences benefit from the additional SNR available at higher field strengths, and can also be used at multiple echo times to form UTE T2* maps. The signal decay in these cases is

often well modeled by a bi-exponential decay curve, with both a short and long component of $T2^*$. Juras *et al.* at the University of Vienna implemented such a sequence at 7 Tesla, and studied the change in both long and short $T2^*$ values of the Achilles tendon in healthy volunteers and people with a history of tendinopathy (14,15). They found significant differences in the short component of $T2^*$ between the two groups ($P < 0.005$), and no significant difference in the long component ($P = 0.99$). Similar $T2^*$ mapping techniques have been demonstrated by Krug *et al.* at the University of California San Francisco in cortical bone at 7 Tesla (16).

Assessment of proteoglycan content in cartilage

Early changes in articular cartilage during the progression of osteoarthritis are not visible in normal radiographs, where changes may only be inferred from the narrowing of joint spacing or gross changes in bone that occur late in the disease (17,18). MRI has been useful for visualizing cartilage directly, allowing earlier detection of morphological changes, yet even these changes are already at a point in the disease where irreversible damage has typically occurred (19). The earliest stages of OA are changes in the cartilage matrix, particularly the depletion of proteoglycans (PG), changes in water content, and molecular level changes in collagen. Early detection of OA would thus require a method of noninvasive measurement of PG concentration and collagen integrity prior to the appearance of any morphological changes (20). With improvements in OA treatments such as cartilage resurfacing procedures and disease modifying drugs, it has become important to develop methods to track the progression of the disease, including the earliest stages, using noninvasive methods.

A variety of noninvasive methods for estimating PG content in cartilage exist in MRI, including delayed gadolinium-enhanced MRI of cartilage (dGEMRIC), T1-rho (or spin-lock MRI) mapping, chemical exchange saturation transfer (CEST) techniques (20), and sodium MRI. The most promising of these for use at 7 Tesla are T1-rho imaging, CEST techniques, and sodium imaging. We review some of the relevant work in each of these areas at 7 Tesla below.

T1-rho imaging

T1-rho mapping is in some ways similar to T2 mapping, but uses low amplitude spin-lock RF pulses after the excitation pulse. This process is repeated with varying spin-

lock pulse time durations (instead of varying echo times, as in T2 mapping). Exponential fitting to this data on a voxel-by-voxel basis produces what are known as T1-rho maps. The contrast is fundamentally different than PD, T1, and T2 contrasts, and describes the relaxation of magnetization in the rotating frame (21). It can be used to study slow *in vivo* interactions between bulk water and surrounding molecules in biological tissues where there is significant motion restriction. The extracellular matrix in cartilage tissue is an example of such an environment, and so changes in this matrix, such as PG depletion, would be reflected by changes in measured T1-rho values (22,23). Early studies in humans indicate elevated T1-rho values among those subjects with OA (24-26).

Some comparisons with traditional imaging methods such as T2 mapping suggest that T1-rho has higher sensitivity to PG depletion in cartilage, although this is not definitively established for human *in vivo* studies with clinically feasible protocols (27-30). T1-rho mapping requires no contrast injection (unlike dGEMRIC) and no additional MRI hardware (unlike sodium). This makes it an attractive candidate for assessing PG content in cartilage.

The spin-lock pulses used in T1-rho deposit significant RF power in the body, so many T1-rho studies are conducted at lower field strengths (1.5 or 3 Tesla). However, a preliminary study by Singh *et al.* demonstrated that concerns over SAR and issues such as B_0 and B_1 inhomogeneity can be overcome at 7T to take advantage of the increased SNR and produce higher resolution (0.2 mm² in-plane resolution) T1-rho maps (31). Wyatt *et al.* also examined the feasibility of relaxation mapping at 7 Tesla, comparing T1-rho to T2 in both normal controls and patients diagnosed with OA as shown in *Figure 5* (32). They found that compared to 3T, imaging at 7 Tesla benefitted from increased SNR and chemical shifts, leading to higher sensitivity to molecular changes at the same resolution and to the detection of more significant regions at 7T. An average improvement of 60 percent in SNR was found, with the SNR calculated in six cartilage compartments shown in *Figure 6* (32). Kogan *et al.* compared T1-rho at 7 Tesla to the gagCEST sequence (described in the next section), and demonstrated good agreement between the two methods (33). Kogan *et al.* also demonstrated a novel method combining the contrast of CEST with T1-rho mapping at 7 Tesla (which they dubbed “CESTrho”) to quantify proton exchange at intermediate exchange rates (34). The method was shown to be insensitive to certain confounding factors such as changes in tissue pH that can alter the exchange rate

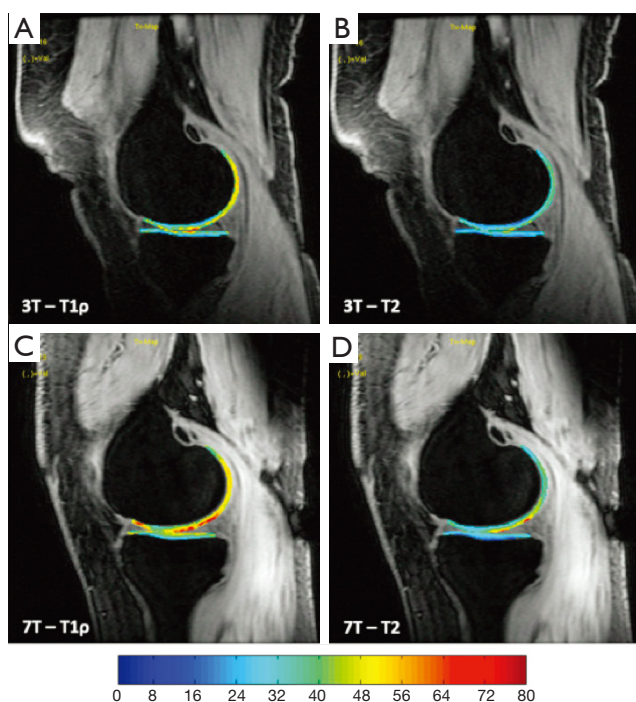


Figure 5 T1-rho and T2 relaxation color maps for the cartilage of the right knee of a healthy volunteer. The top row depicts a T1-rho map overlaid on a 3D-FSE anatomical image (A) and a T2 map overlaid on a 3D-FSE anatomical image (B) at 3T. The bottom row depicts the corresponding images and maps at 7T. The color maps have the same scale, displayed in milliseconds (32). Note the overall uniformity of the maps and spatial similarity between 3T and 7T. The 7 Tesla maps also appear to indicate a larger range of values across the cartilage for both T1-rho and T2, although future work is needed to more fully explain the differences observed. (Reproduced from Wyatt C, Guha A, Venkatachari A, Li X, Krug R, Kelley DE, Link T, Majumdar S. Improved differentiation between knees with cartilage lesions and controls using 7T relaxation time mapping. *J Orthop Translat* 2015;3:197-204.)

of protons.

Chemical exchange saturation transfer (CEST)

CEST is a noninvasive molecular imaging technique. It functions by measuring the exchange of protons in a larger molecule with a much larger pool of protons in the surrounding water. CEST agents are molecules that have exchangeable protons. Protons in the molecules of a CEST agent have a different resonant RF frequency compared to water, so a selective RF pulse can be applied to saturate the signal from these molecules, equalizing the number of spins aligned parallel and antiparallel to the main magnetic

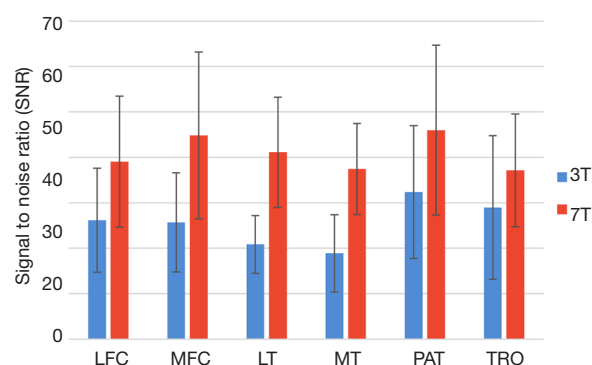


Figure 6 Wyatt *et al.* examined the feasibility of relaxation mapping at 7 Tesla, comparing T1-rho to T2 in both normal controls and patients diagnosed with OA. They found that compared to 3T, imaging at 7 Tesla benefitted from an average SNR improvement of 60% and larger chemical shifts, leading to higher sensitivity to molecular changes at the same resolution. The improvement in SNR was calculated in six cartilage compartments at 3T and 7T. LFC, lateral femoral condyle; LT, lateral tibial; MFC, medial femoral condyle; MT, medial tibial; PAT, patella; TRO, trochlea (32). (Reproduced from Wyatt C, Guha A, Venkatachari A, Li X, Krug R, Kelley DE, Link T, Majumdar S. Improved differentiation between knees with cartilage lesions and controls using 7T relaxation time mapping. *J Orthop Translat* 2015;3:197-204.)

field. These saturated protons are then exchanged with unsaturated protons in the surrounding water causing a decrease in the signal proportional to the concentration of the CEST agent present (35). The CEST effect has been shown to be sensitive to concentration of PG content in cartilage (36,37). A further advantage is that, like T1-rho, CEST sequences don't require specialized hardware or contrast agent injection. However, CEST sequences require significant post-processing, as described below.

A typical CEST mapping protocol consists of a number of steps. First, CEST images are collected by applying saturation pulses over a range of different chemical shifts in a series of images. After the initial saturation, water is imaged using a traditional sequence such as a GRE sequence (35). Since direct saturation effects that saturate a portion of the water protons may cause an asymmetry in the water signal, often images with saturation pulses both above and below the water resonance are acquired to remove this asymmetry later in analysis. An additional image with no saturation is also acquired for a baseline comparison. In addition, B_0 and B_1 maps are often acquired to correct for any B_0 and B_1 inhomogeneity (37). After correcting for

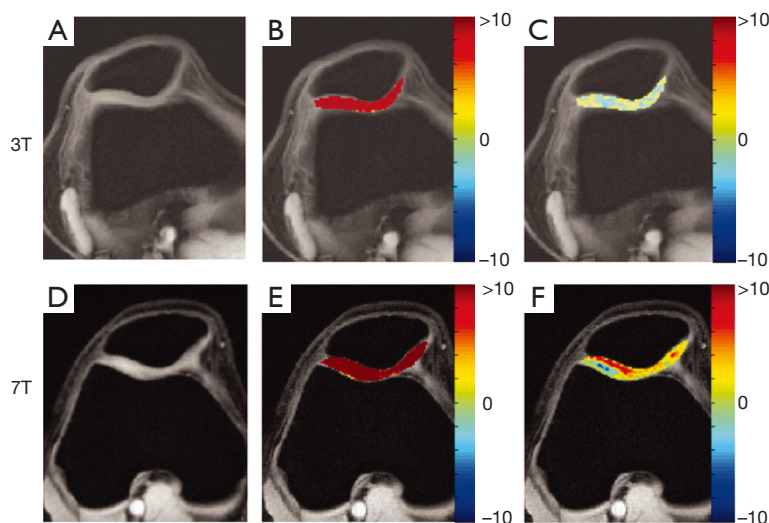


Figure 7 Top row depicts a fat suppressed anatomical image of knee cartilage (A), that image with a gagCEST map overlaid that is either uncorrected (B) or corrected (C) for B_0 inhomogeneity at 3T. The corresponding images and gagCEST maps at 7T are shown in (D)-(F) on the bottom row. Numbers for the gagCEST maps indicate percentage signal change compared to baseline. Note that prior to B_0 correction, gagCEST values in both cases are greater than 10%, while after correction values at 3T are negligible but at 7T are still about 6% (38). (Copyright 2012 Wiley. Used with permission from Singh A, Haris M, Cai K, Kassey VB, Kogan F, Reddy D, Hariharan H, Reddy R. Chemical exchange saturation transfer magnetic resonance imaging of human knee cartilage at 3 T and 7 T. *Magn Reson Med* 2012;68:588-94.)

these effects, the signal with applied saturation below the water resonance is subtracted from the corresponding signal with saturation applied above the water resonance, and then compared to the baseline signal with no saturation (36). The CEST effect is thus given as a percentage of the baseline signal.

Ling *et al.* developed a CEST sequence sensitive to PG content, which they termed gagCEST (36). A study conducted by Singh *et al.* at the University of Pennsylvania demonstrated the benefits of performing CEST studies at 7T by comparing results in knee cartilage at both 3T and 7T (38). After making corrections for B_0 inhomogeneity, only negligible gagCEST values could be measured at 3T while at 7T a significant effect of about 6 percent remained. At 7T the larger chemical shift and higher SNR produce much more promising results, as shown in *Figure 7* (38). Studies conducted by Schmitt *et al.* compared results from gagCEST at 7T to sodium imaging in patients after cartilage repair surgery and demonstrated high correlation between gagCEST and sodium concentrations, indicating that gagCEST holds promise as a biomarker for PG content (39,40). A study at 7T and at 11.7T by Ling, Saar, *et al.* demonstrated that gagCEST can also be used to determine glycosaminoglycan (GAG) concentration in the

intervertebral discs in ex vivo porcine samples that had been prepared with various known GAG concentrations (41,42). They also confirmed that GAG concentration determined using gagCEST correlated with concentrations determined using sodium images (42). gagCEST is a particularly promising method for tracking intervertebral disc health since contrast based methods such as dGEMRIC are ineffective in the discs. Krishnamoorthy *et al.* introduced a new magnetization prepared 3D GRE gagCEST sequence, improving on the achievable contrast and reducing total acquisition time for the protocol to something clinically practical (43). Kogan *et al.* developed a multislice gagCEST acquisition to reduce scan times and enhance the clinical viability of gagCEST (33).

The exchange of protons in the amine group of creatine (Cr) is also potentially interesting for quantitative MSK imaging. Cr plays a crucial role in the storage and transmission of phosphate bound energy in muscle. During exercise, phosphocreatine is depleted to maintain the supply of adenosine triphosphate leading to a surplus Cr concentration. Cr also exchanges protons with surrounding bulk water and its amine group, thus exhibiting a CEST effect. Haris *et al.* demonstrated a CrCEST map at 7T in resting calf muscle of a healthy human volunteer (44).

Dynamic response to exercise was demonstrated at 7 Tesla by Kogan *et al.* in human calf muscle of 8 healthy volunteers before and after plantar flexion exercise (45). A variety of other musculoskeletal studies using CrCEST at 7 Tesla can be found in (46,47).

Sodium MRI

While all of the above techniques are based on the NMR signal from the ^1H nucleus in tissues, it is also possible to form MRI images from other nuclei, such as ^{23}Na (sodium) (48). However, each nucleus has a unique characteristic frequency of the NMR signal (called the Larmor frequency). The Larmor frequency for sodium (^{23}Na) at 7 Tesla is ~ 79 MHz, or roughly one quarter that of hydrogen. This translates into a sodium NMR signal wavelength that is roughly four times as long as that of hydrogen. As a consequence, custom radiofrequency hardware is needed to produce sodium MRI images. This includes custom transmit and receive RF coils tuned to the sodium Larmor frequency, as well as RF signal generators and amplifiers capable of operating at the sodium Larmor frequency. These components are typically available as options from the major MR vendors, and a variety of third party vendors will build custom sodium-tuned coils for various applications. A positive consequence of the longer sodium NMR signal wavelength is that sodium MRI at 7 Tesla doesn't suffer from many of the wavelength-related issues previously outlined that apply to hydrogen imaging at 7 Tesla. In fact, in many respects the radiofrequency considerations for sodium imaging at 7 Tesla are similar to those of hydrogen at 1.5 Tesla. (Note that power deposition, or SAR, can still be a problem with sodium imaging at 7 Tesla, but this is typically easily manageable given the pulse sequences commonly used for sodium imaging. There is little to no advantage in using RF heating-intensive sequences such as fast spin echo for sodium MRI, so SAR generally is not an issue.)

The much lower prevalence of sodium in the human body *vs.* hydrogen and the lower magnetic polarization achieved in sodium *vs.* hydrogen at a given field strength lead to very low sodium signal levels, and *in vivo* sodium MR images tend to be noisy even at poor resolutions (isotropic resolutions of several millimeters) and long scan times (greater than 15 minutes). The additional potential SNR from a higher polarizing field, coupled with the diminished concerns arising from RF wavelength issues, make sodium MRI a very attractive option on ultra high field systems to mitigate some of these difficulties.

The clinical motivation for sodium MRI for musculoskeletal applications stems from the fact that sodium concentrations in the body reveal completely different physiological information than traditional hydrogen imaging. In cartilage, the concentration of sodium is linearly related to the concentration of proteoglycan (PG) (49-52). Quantitative measurement of the sodium concentration in cartilage via MRI can thus serve as a direct proxy for PG content, potentially allowing the detection of very early degenerative changes in cartilage that portend the onset of osteoarthritis (as discussed for both T1-rho and gagCEST imaging above). Other musculoskeletal applications of quantitative sodium MRI, which could all benefit from the higher SNR achievable at 7 Tesla, include imaging of sodium concentrations in muscle [for assessment of muscular dystrophies and channelopathies (53-58), and muscle response to exercise (59-62)], imaging of sodium concentrations in tendon (14), and even assessment of intervertebral disc health (63,64).

Figure 8 shows 7 Tesla sodium imaging for both cartilage (A-D) and tendon (E,F). In the top two rows of *Figure 8*, an illustration of potentially age-related changes in PG content in patellar cartilage is shown. The proton images of a healthy 35-year-old (A) and a healthy 64-year-old (C) both reveal morphologically healthy cartilage. The sodium images (both shown on the same color scale) reveal an apparent significant decrease in PG content in the 64-year-old (D) *vs.* the 35-year old (B). A comparison of sagittal sodium scans from Juras *et al.* at 7 Tesla of the Achilles tendon are shown in (E) for a healthy 27-year-old control and (F) for a 46-year-old with chronic Achilles tendinopathy. A distinct increase in sodium signal in the subject with tendinopathy is clearly evident in these images.

Diffusion tensor imaging

Diffusion tensor imaging (DTI) has been suggested as a means of both probing cartilage matrix integrity and structure (through fractional anisotropy, or FA), and potentially assessing proteoglycan content (through mean apparent diffusion coefficient, or ADC) (65-68). However, the long echo times typically required for traditional DTI and the relatively short echo times of cartilage have made DTI in cartilage at 1.5 and 3 Tesla impractical due to low signal and prohibitively long scan times.

Filidoro *et al.* in Munich, Germany demonstrated the feasibility of using high field (9.4 Tesla) DTI in evaluating

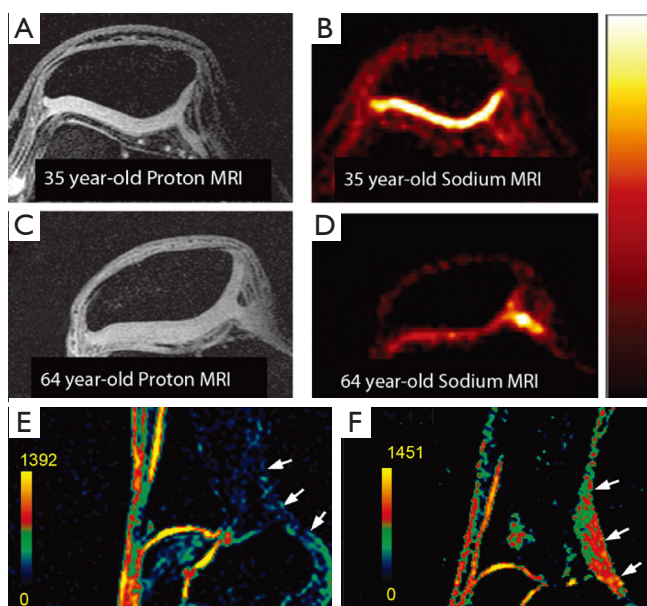


Figure 8 In (A-D), a demonstration of potentially age-related changes in proteoglycan content as revealed by high-resolution (1 mm × 1 mm × 2 mm, 26 minute total scan time) sodium MRI at 7 Tesla using a 3D cones sodium imaging sequence. While the cartilage looks healthy on both subjects in the proton images (A) and (C), there is a marked apparent decrease in sodium signal in the older subject (D) *vs.* the younger subject (B). In (E) and (F), Juras *et al.* show sodium 7T scans of the Achilles tendon from a healthy 27-year-old control (E), and a 46-year-old with chronic Achilles tendinopathy (F). A distinct increase in sodium signal in the subject with tendinopathy is clearly evident in these images (14). (A-D) used courtesy of Stanford University Department of Radiology. (E) and (F) Copyright The Radiological Society of North America. (Reproduced with permission from Juras V, Zbýň Š, Pressl C, Domayer SE, Hofstaetter JG, Mayerhoefer ME, Windhager R, Trattng S. Sodium MR imaging of Achilles tendinopathy at 7 T: preliminary results. *Radiology* 2012;262:199-205.)

hyaline cartilage structure from excised *ex vivo* human patellae (68). Note that this work was performed on a small animal machine, but is nevertheless an interesting application of ultra high-field quantitative musculoskeletal MRI. They utilized a diffusion-weighted pulsed gradient spin echo sequence, and acquired 12 separate diffusion directions. They were able to observe changes in fractional anisotropy (FA) and mean diffusivity with depth in cartilage from the superficial to deep radial zones, presumably corresponding to changes in collagen matrix fibril structure

and direction across these regions.

Raya *et al.* at New York University used a line-scan DTI imaging sequence at 7 Tesla to compare articular cartilage in healthy subjects to those with osteoarthritis (69). They found that mean ADC and FA values were both good differentiators between the two groups, with mean ADC having higher specificity. Examples of ADC, FA and T2 maps for three patients (one healthy control and two with OA) can be seen in *Figure 9*. Large differences between the healthy volunteer and the osteoarthritic patients are observed, particularly in ADC.

Discussion and conclusion

As can be seen, there has been significant work on the development of quantitative musculoskeletal imaging techniques at 7 Tesla for a variety of applications. We have outlined what we believe to be some of the most promising techniques in the relative near term. These include ultra-high resolution 3D morphological sequences, techniques for assessing trabecular bone microarchitecture, various T2 and T2* mapping techniques (including several novel steady-state model-based 3D T2 mapping techniques), several promising techniques for assessing proteoglycan content in cartilage (T1-rho mapping, gagCEST, and sodium MRI), and diffusion tensor imaging in cartilage.

The resolution and contrast that can be achieved with several of the ultra-high resolution 3D morphological sequences at 7 Tesla shown in the knee is very promising. When this data is compared to data from the 10 minute 3D DESS scan protocol from the OAI, it seems probable that the additional resolution, SNR, and enhanced contrast of the 7 Tesla protocols may further improve both ease of morphological segmentation and the accuracy and repeatability of quantitative measurements of cartilage volume and thickness. Studies are needed in the coming years to demonstrate if this is indeed the case.

While T2 mapping has been performed at 7 Tesla using standard 2D MESE sequences (as shown above), these sequences do suffer from flip angle inhomogeneity, high SAR (tissue heating) due to refocusing pulses for the spin echoes, and they can't easily be extended to 3D in reasonable scan times. Several of the new steady state sequences, such as 3D-TESS and 3D quantitative DESS, are quite promising. They can provide full volume 3D T2 maps at relatively high resolutions, and are often extracted from images of sufficient quality for making morphological measurements. We expect to see these sequences become

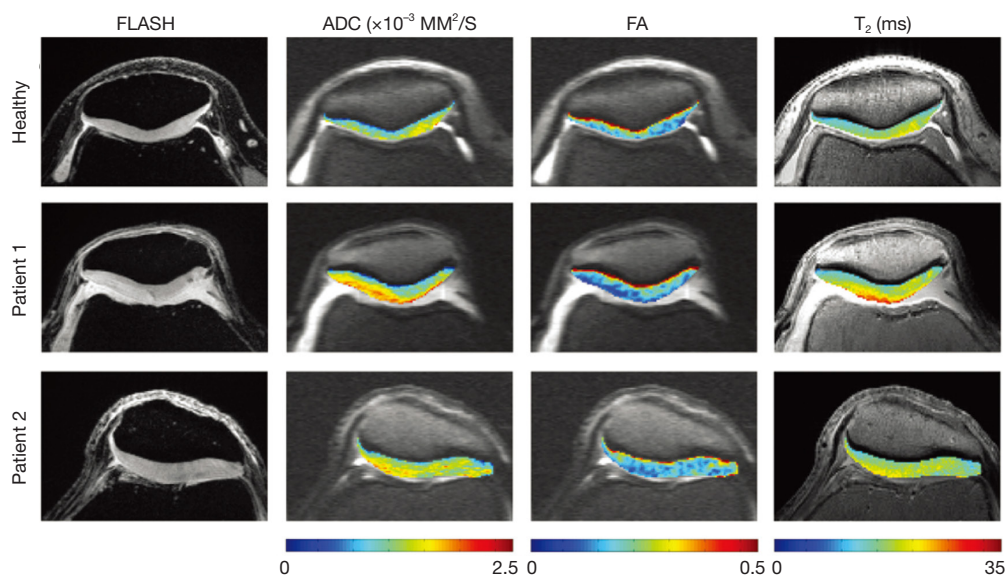


Figure 9 Raya *et al.* at New York University used a line-scan DTI imaging sequence at 7 Tesla to compare articular cartilage in healthy subjects to those with osteoarthritis. Comparison of apparent diffusion coefficient (ADC), fractional anisotropy (FA), and T2 maps between one healthy volunteer (31-year-old man right knee) and two patients diagnosed with osteoarthritis (patient 1: 60-year-old woman with Kellgren-Lawrence grade 3 right knee; patient 2: 64-year-old man with Kellgren-Lawrence grade 2 left knee). Although both ADC and FA showed significant differences between the healthy population and the osteoarthritic population, the differences between ADC values are more clear (69). Copyright Radiological Society of North America. (Reproduced with permission from Raya JG, Horng A, Dietrich O, Krasnokutsky S, Beltran LS, Storey P, Reiser MF, Recht MP, K. Sodickson D, Glaser C. Articular cartilage: in vivo diffusion-tensor imaging. *Radiology* 2012;262:550-9.)

more common in musculoskeletal imaging, combining high resolution morphological scanning with full 3D T2 maps. This is particularly feasible at 7 Tesla, where the high SNR makes the model-based estimation of T2 more robust at high resolutions.

We believe that ultra-high resolution 3D morphological scanning coupled with model-based relaxometry measurements derived from the same sequence could become a standard for imaging of cartilage at 7 Tesla. When such a sequence is combined with one of the several techniques available at 7 Tesla for assessment of PG content in cartilage (T1-rho, gagCEST, or sodium), it appears possible to have an *in vivo* 7 Tesla protocol for joint imaging that provides unprecedented resolution and contrast for morphological assessment of the joint, coupled with 3D T2 maps and a 3D sequence sensitive to PG content in an exam of approximately 30 minutes duration.

One major drawback for musculoskeletal imaging at 7 Tesla, however, is the difficulty in achieving a homogeneous excitation and homogeneous signal reception across large

fields of view, and in particular across sections of the anatomy on the torso (which can't be surrounded by a small birdcage transmit coil). While coils such as that shown in *Figure 1* are under development for imaging the hip and spine, it isn't clear that such coils will be efficient enough to compete with protocols at lower field strengths. We are thus less optimistic about the future of musculoskeletal imaging at 7 Tesla for regions of the body other than the knee, other peripheral joints, and superficial areas that can be easily imaged with simple surface coils. Indeed, the preponderance of musculoskeletal work at 7 Tesla that focuses on the knee or other small joints indicates that imaging of other areas, such as the hip, is still very much an open research challenge.

Acknowledgements

The authors wish to acknowledge and thank the Southampton Football Club for their support of imaging studies at the University of Oxford. Imaging studies at the University of Oxford were also supported by a

generous grant from Oxfordshire Health Services Research Committee (Reference 1134).

Footnote

Conflicts of Interest: The authors have no conflicts of interest to declare.

References

- Siemens AG. New 7 Tesla MRI research system ready for future clinical use. 2015. Available online: <http://www.siemens.com/press/PR2015060231HCEN>
- Collins CM, Wang Z. Calculation of radiofrequency electromagnetic fields and their effects in MRI of human subjects. *Magn Reson Med* 2011;65:1470-82.
- Nevitt MC, Felson DT, Lester G. The Oseoarthritis Initiative: Protocol for the Cohort Study. 1.1 ed. 2006.
- Chang G, Pakin SK, Schweitzer ME, Saha PK, Regatte RR. Adaptations in trabecular bone microarchitecture in Olympic athletes determined by 7T MRI. *J Magn Reson Imaging* 2008;27:1089-95.
- Chang G, Wang L, Liang G, Babb JS, Saha PK, Regatte RR. Reproducibility of subregional trabecular bone micro-architectural measures derived from 7-Tesla magnetic resonance images. *MAGMA* 2011;24:121-5.
- Chang G, Xia D, Sherman O, Strauss E, Jazrawi L, Recht MP, Regatte RR. High resolution morphologic imaging and T2 mapping of cartilage at 7 Tesla: comparison of cartilage repair patients and healthy controls. *MAGMA* 2013;26:539-48.
- Menezes NM, Gray ML, Hartke JR, Burstein D. T2 and T1rho MRI in articular cartilage systems. *Magn Reson Med* 2004;51:503-9.
- Welsch GH, Apprich S, Zbyn S, Mamisch TC, Mlynarik V, Scheffler K, Bieri O, Trattnig S. Biochemical (T2, T2* and magnetisation transfer ratio) MRI of knee cartilage: feasibility at ultra-high field (7T) compared with high field (3T) strength. *Eur Radiol* 2011;21:1136-43.
- Lazik A, Theysohn JM, Geis C, Johst S, Ladd ME, Quick HH, Kraff O. 7 Tesla quantitative hip MRI: T1, T2 and T2* mapping of hip cartilage in healthy volunteers. *Eur Radiol* 2016;26:1245-53.
- Domayer SE, Apprich S, Stelzeneder D, Hirschfeld C, Sokolowski M, Kronnerwetter C, Chiari C, Windhager R, Trattnig S. Cartilage repair of the ankle: first results of T2 mapping at 7.0 T after microfracture and matrix associated autologous cartilage transplantation. *Osteoarthritis Cartilage* 2012;20:829-36.
- Kraff O, Lazik-Palm A, Heule R, Theysohn JM, Bieri O, Quick HH. 7 Tesla quantitative hip MRI: a comparison between TESS and CPMG for T2 mapping. *MAGMA* 2016;29:503-12.
- Juras V, Zbýň Š, Mlynarik V, Szomolanyi P, Hager B, Baer P, Frollo I, Trattnig S. The compositional difference between ankle and knee cartilage demonstrated by T2 mapping at 7 Tesla MR. *Eur J Radiol* 2016;85:771-7.
- Staroswiecki E, Granlund KL, Alley MT, Gold GE, Hargreaves BA. Simultaneous estimation of T(2) and apparent diffusion coefficient in human articular cartilage in vivo with a modified three-dimensional double echo steady state (DESS) sequence at 3 T. *Magn Reson Med* 2012;67:1086-96.
- Juras V, Zbyn S, Pressl C, Domayer SE, Hofstaetter JG, Mayerhoefer ME, Windhager R, Trattnig S. Sodium MR imaging of Achilles tendinopathy at 7 T: preliminary results. *Radiology* 2012;262:199-205.
- Juras V, Zbyn S, Pressl C, Valkovic L, Szomolanyi P, Frollo I, Trattnig S. Regional variations of T2* in healthy and pathologic achilles tendon in vivo at 7 Tesla: preliminary results. *Magn Reson Med* 2012;68:1607-13.
- Krug R, Larson PE, Wang C, Burghardt AJ, Kelley DA, Link TM, Zhang X, Vigneron DB, Majumdar S. Ultrashort echo time MRI of cortical bone at 7 tesla field strength: a feasibility study. *J Magn Reson Imaging* 2011;34:691-5.
- Boegård T, Rudling O, Petersson IF, Jonsson K. Correlation between radiographically diagnosed osteophytes and magnetic resonance detected cartilage defects in the tibiofemoral joint. *Ann Rheum Dis* 1998;57:401-7.
- Kijowski R, Blankenbaker DG, Stanton PT, Fine JP, De Smet AA. Radiographic findings of osteoarthritis versus arthroscopic findings of articular cartilage degeneration in the tibiofemoral joint. *Radiology* 2006;239:818-24.
- Chan WP, Lang P, Stevens MP, Sack K, Majumdar S, Stoller DW, Basch C, Genant HK. Osteoarthritis of the knee: comparison of radiography, CT, and MR imaging to assess extent and severity. *AJR Am J Roentgenol* 1991;157:799-806.
- Matzat SJ, Kogan F, Fong GW, Gold GE. Imaging strategies for assessing cartilage composition in osteoarthritis. *Curr Rheumatol Rep* 2014;16:462.
- Redfield AG. Nuclear Magnetic Resonance Saturation and Rotary Saturation in Solids. *Phys Rev* 1955;98:1787-809.
- Akella SV, Regatte RR, Gougoutas AJ, Borthakur A, Shapiro

- EM, Kneeland JB, Leigh JS, Reddy R. Proteoglycan-induced changes in T1rho-relaxation of articular cartilage at 4T. *Magn Reson Med* 2001;46:419-23.
23. Regatte RR, Akella SV, Borthakur A, Kneeland JB, Reddy R. In vivo proton MR three-dimensional T1rho mapping of human articular cartilage: initial experience. *Radiology* 2003;229:269-74.
 24. Duvvuri U, Reddy R, Patel SD, Kaufman JH, Kneeland JB, Leigh JS. T1rho-relaxation in articular cartilage: effects of enzymatic degradation. *Magn Reson Med* 1997;38:863-7.
 25. Matzat SJ, van Tiel J, Gold GE, Oei EH. Quantitative MRI techniques of cartilage composition. *Quant Imaging Med Surg* 2013;3:162-74.
 26. Wang YX, Zhang Q, Li X, Chen W, Ahuja A, Yuan J. T1ρ magnetic resonance: basic physics principles and applications in knee and intervertebral disc imaging. *Quant Imaging Med Surg* 2015;5:858-85.
 27. Regatte RR, Akella SV, Borthakur A, Kneeland JB, Reddy R. Proteoglycan depletion-induced changes in transverse relaxation maps of cartilage: comparison of T2 and T1rho. *Acad Radiol* 2002;9:1388-94.
 28. Regatte RR, Akella SV, Lonner JH, Kneeland JB, Reddy R. T1rho relaxation mapping in human osteoarthritis (OA) cartilage: comparison of T1rho with T2. *J Magn Reson Imaging* 2006;23:547-53.
 29. Li X, Benjamin Ma C, Link TM, Castillo DD, Blumenkrantz G, Lozano J, Carballido-Gamio J, Ries M, Majumdar S. In vivo T(1rho) and T(2) mapping of articular cartilage in osteoarthritis of the knee using 3 T MRI. *Osteoarthritis Cartilage* 2007;15:789-97.
 30. van Tiel J, Kotek G, Reijman M, Bos PK, Bron EE, Klein S, Nasserinejad K, van Osch GJ, Verhaar JA, Krestin GP, Weinans H, Oei EH. Is T1ρ Mapping an Alternative to Delayed Gadolinium-enhanced MR Imaging of Cartilage in the Assessment of Sulphated Glycosaminoglycan Content in Human Osteoarthritic Knees? An in Vivo Validation Study. *Radiology* 2016;279:523-31.
 31. Singh A, Haris M, Cai K, Kogan F, Hariharan H, Reddy R. High resolution T1ρ mapping of in vivo human knee cartilage at 7T. *PLoS One* 2014;9:e97486.
 32. Wyatt C, Guha A, Venkatachari A, Li X, Krug R, Kelley DE, Link T, Majumdar S, et al. Improved differentiation between knees with cartilage lesions and controls using 7T relaxation time mapping. *J Orthop Translat* 2015;3:197-204.
 33. Kogan F, Hargreaves BA, Gold GE. Volumetric multislice gagCEST imaging of articular cartilage: Optimization and comparison with T1rho. *Magn Reson Med* 2016. [Epub ahead of print].
 34. Kogan F, Singh A, Cai K, Haris M, Hariharan H, Reddy R. Investigation of chemical exchange at intermediate exchange rates using a combination of chemical exchange saturation transfer (CEST) and spin-locking methods (CESTRho). *Magn Reson Med* 2012;68:107-19.
 35. van Zijl PC, Yadav NN. Chemical exchange saturation transfer (CEST): what is in a name and what isn't? *Magn Reson Med* 2011;65:927-48.
 36. Ling W, Regatte RR, Navon G, Jerschow A. Assessment of glycosaminoglycan concentration in vivo by chemical exchange-dependent saturation transfer (gagCEST). *Proc Natl Acad Sci U S A* 2008;105:2266-70.
 37. Kogan F, Hariharan H, Reddy R. Chemical Exchange Saturation Transfer (CEST) Imaging: Description of Technique and Potential Clinical Applications. *Curr Radiol Rep* 2013;1:102-114.
 38. Singh A, Haris M, Cai K, Kasse VB, Kogan F, Reddy D, Hariharan H, Reddy R. Chemical exchange saturation transfer magnetic resonance imaging of human knee cartilage at 3 T and 7 T. *Magn Reson Med* 2012;68:588-94.
 39. Schmitt B, Zbyn S, Stelzener D, Jellus V, Paul D, Lauer L, Bachert P, Trattning S. Cartilage quality assessment by using glycosaminoglycan chemical exchange saturation transfer and (23)Na MR imaging at 7 T. *Radiology* 2011;260:257-64.
 40. Krusche-Mandl I, Schmitt B, Zak L, Apprich S, Aldrian S, Juras V, Friedrich KM, Marlovits S, Weber M, Trattning S. Long-term results 8 years after autologous osteochondral transplantation: 7 T gagCEST and sodium magnetic resonance imaging with morphological and clinical correlation. *Osteoarthritis Cartilage* 2012;20:357-63.
 41. Ling W, Saar G, Regatte RR, Jerschow A, Navon G, editors. Assessing the Intervertebral Disc via gagCEST. *Proceedings of the International Society for Magnetic Resonance in Medicine*; 2009; Honolulu, HI. Available online: <http://cds.ismrm.org/protected/09MProceedings/files/00293.pdf>
 42. Saar G, Zhang B, Ling W, Regatte RR, Navon G, Jerschow A. Assessment of glycosaminoglycan concentration changes in the intervertebral disc via chemical exchange saturation transfer. *NMR Biomed* 2012;25:255-61.
 43. Krishnamoorthy G, Nanga RP, Bagga P, Hariharan H, Reddy R. High quality three-dimensional gagCEST imaging of in vivo human knee cartilage at 7 tesla. *Magn Reson Med* 2016. [Epub ahead of print].

44. Haris M, Cai K, Singh A, KC VB, Hariharan H, Reddy R, editors. Chemical Exchange Saturation Transfer effect from Phospho-creatine (PCr) and Adeno-sine-triphosphate (ATP) Proceedings of the International Society for Magnetic Resonance in Medicine; 2011; Montréal, Québec, Canada. Available online: <http://cds.ismrm.org/protected/11MProceedings/files/2767.pdf>
45. Kogan F, Haris M, Singh A, Cai K, Debrosse C, Nanga RP, Hariharan H, Reddy R. Method for high-resolution imaging of creatine in vivo using chemical exchange saturation transfer. *Magn Reson Med* 2014;71:164-72.
46. Kogan F, Stafford RB, Englund EK, Gold GE, Hariharan H, Detre JA, Reddy R. Perfusion has no effect on the in vivo CEST effect from Cr (CrCEST) in skeletal muscle. *NMR Biomed* 2017;30. doi: 10.1002/nbm.3673.
47. Kogan F, Haris M, Debrosse C, Singh A, Nanga RP, Cai K, Hariharan H, Reddy R. In vivo chemical exchange saturation transfer imaging of creatine (CrCEST) in skeletal muscle at 3T. *J Magn Reson Imaging* 2014;40:596-602.
48. Bangerter NK, Tarbox GJ, Taylor MD, Kaggie JD. Quantitative sodium magnetic resonance imaging of cartilage, muscle, and tendon. *Quant Imaging Med Surg* 2016;6:699-714.
49. Reddy R, Insko EK, Noyszewski EA, Dandora R, Kneeland JB, Leigh JS. Sodium MRI of human articular cartilage in vivo. *Magn Reson Med* 1998;39:697-701.
50. Shapiro EM, Borthakur A, Gougoutas A, Reddy R. ²³Na MRI accurately measures fixed charge density in articular cartilage. *Magn Reson Med* 2002;47:284-91.
51. Insko EK, Kaufman JH, Leigh JS, Reddy R. Sodium NMR evaluation of articular cartilage degradation. *Magn Reson Med* 1999;41:30-4.
52. Wheaton AJ, Borthakur A, Dodge GR, Kneeland JB, Schumacher HR, Reddy R. Sodium magnetic resonance imaging of proteoglycan depletion in an in vivo model of osteoarthritis. *Acad Radiol* 2004;11:21-8.
53. Vilin YY, Ruben PC. Slow inactivation in voltage-gated sodium channels: molecular substrates and contributions to channelopathies. *Cell Biochem Biophys* 2001;35:171-90.
54. Amarteifio E, Nagel A, Weber M-A, Jurkat-Rott K, Lehmann-Horn F. Evaluation of Myoplasmic Sodium in Hyperkalemic Periodic Paralysis with 3Tesla Magnetic Resonance Imaging. *Klin Neurophysiol* 2012;43:228-32.
55. Amarteifio E, Nagel AM, Weber MA, Jurkat-Rott K, Lehmann-Horn F. Hyperkalemic periodic paralysis and permanent weakness: 3-T MR imaging depicts intracellular ²³Na overload--initial results. *Radiology* 2012;264:154-63.
56. Nagel AM, Amarteifio E, Lehmann-Horn F, Jurkat-Rott K, Semmler W, Schad LR, Weber MA. 3 Tesla sodium inversion recovery magnetic resonance imaging allows for improved visualization of intracellular sodium content changes in muscular channelopathies. *Invest Radiol* 2011;46:759-66.
57. Weber MA, Nagel AM, Jurkat-Rott K, Lehmann-Horn F. Sodium (²³Na) MRI detects elevated muscular sodium concentration in Duchenne muscular dystrophy. *Neurology* 2011;77:2017-24.
58. Weber MA, Nagel AM, Wolf MB, Jurkat-Rott K, Kauczor HU, Semmler W, Lehmann-Horn F. Permanent muscular sodium overload and persistent muscle edema in Duchenne muscular dystrophy: a possible contributor of progressive muscle degeneration. *J Neurol* 2012;259:2385-92.
59. Chang G, Wang L, Schweitzer ME, Regatte RR. 3D ²³Na MRI of human skeletal muscle at 7 Tesla: initial experience. *Eur Radiol* 2010;20:2039-46.
60. Bansal N, Szczepaniak L, Ternullo D, Fleckenstein JL, Malloy CR. Effect of exercise on (²³Na) MRI and relaxation characteristics of the human calf muscle. *J Magn Reson Imaging* 2000;11:532-8.
61. Hammon M, Grossmann S, Linz P, Kopp C, Dahlmann A, Janka R, Cavallaro A, Uder M, Titze J. 3 Tesla (²³Na) magnetic resonance imaging during aerobic and anaerobic exercise. *Acad Radiol* 2015;22:1181-90.
62. Constantinides CD, Gillen JS, Boada FE, Pomper MG, Bottomley PA. Human skeletal muscle: sodium MR imaging and quantification--potential applications in exercise and disease. *Radiology* 2000;216:559-68.
63. Ooms KJ, Cannella M, Vega AJ, Marcolongo M, Polenova T. ²³Na TQF NMR imaging for the study of spinal disc tissue. *J Magn Reson* 2008;195:112-5.
64. Insko EK, Clayton DB, Elliott MA. In vivo sodium MR imaging of the intervertebral disk at 4 T. *Acad Radiol* 2002;9:800-4.
65. Meder R, de Visser SK, Bowden JC, Bostrom T, Pope JM. Diffusion tensor imaging of articular cartilage as a measure of tissue microstructure. *Osteoarthritis Cartilage* 2006;14:875-81.
66. Deng X, Farley M, Nieminen MT, Gray M, Burstein D. Diffusion tensor imaging of native and degenerated human articular cartilage. *Magn Reson Imaging* 2007;25:168-71.
67. de Visser SK, Bowden JC, Wentrup-Byrne E, Rintoul L, Bostrom T, Pope JM, Momot KI. Anisotropy of

- collagen fibre alignment in bovine cartilage: comparison of polarised light microscopy and spatially resolved diffusion-tensor measurements. *Osteoarthritis Cartilage* 2008;16:689-97.
68. Filidoro L, Dietrich O, Weber J, Rauch E, Oerther T, Wick M, Reiser MF, Glaser C. High-resolution diffusion tensor imaging of human patellar cartilage: feasibility and preliminary findings. *Magn Reson Med* 2005;53:993-8.
69. Raya JG, Horng A, Dietrich O, Krasnokutsky S, Beltran LS, Storey P, Reiser MF, Recht MP, Sodickson DK, Glaser C. Articular cartilage: in vivo diffusion-tensor imaging. *Radiology* 2012;262:550-9.

Cite this article as: Bangerter NK, Taylor MD, Tarbox GJ, Palmer AJ, Park DJ. Quantitative techniques for musculoskeletal MRI at 7 Tesla. *Quant Imaging Med Surg* 2016;6(6):715-730. doi: 10.21037/qims.2016.12.12